Objective: Quantitative ultrasound is now used in the clinic for the estimation of bone quality. However, the interaction between an ultrasonic wave and bone tissue remains unclear. A transient ultrasonic wave propagating in cancellous bone has been shown to separates into two waves, referred to as fast wave and slow wave, respectively.
The frequency of the fast wave is lower than that of the slow wave and the wave may last longer depending on the condition of bone specimen. These characteristics of fast wave has been interpreted as the effect of its discriminating propagation path, which is mainly inside the solid part (trabeculae) of cancellous bone. However, few precise investigations of the effect of propagation path of the fast wave has been performed because it was difficult to be evidenced experimentally.
Methods: In this study, we performed three-dimensional numerical simulations using numerical models of actual bone specimens. In order to understand the mechanism explaining the properties of the fast wave, we focused on the spatial distribution of propagating waves in cancellous bone. In the simulations, various configurations of wave propagation were simulated by artificially changing the spatial location and the planar dimension of the receiver and the thickness of the specimen.
Results: The waveforms received by the various sized sensors (from a point-sized sensor to 15x15 square-millimeter sensor) are recorded. The result showed that the shape and the temporal characteristics of the received waves varied widely depending on the location, which may be caused by not only the bone density around the propagating area but also the bone structure (alignment and connection of trabeculae). Hence, this incoherence of the waves strongly lowers the frequency of fast wave when the wave was received by a planar sensor. Although it is sure that the frequency of the waveform received by a point sensor was lower than that of transmitted wave, which may be caused by the multiple reflection inside cancellous bone, the results of the simulation showed that the effect of the surface integral on the planar sensor is also not negligible.
Conclusion: The effect of spatial distribution of bone structure should be considered in practical bone assessments using quantitative ultrasound.

IBDW2014-00165-F0086
IMPACT OF AXIAL TRANSMISSION ULTRASOUND AND BONE MINERAL DENSITY ON THE BREAKING STRENGTH OF CORTICAL CUBOID BONE SAMPLES

Reinhard Barkmann [a], Melanie Daugschies [a], Kay Raum [b], Robert Wendlandt [c], Pascal Laugier [d], Qentin Grimal [d], Claus-C. Glüer [a]
[a]*Section Biomedical Imaging, Department of Radiology and Neuroradiology, University Hospital Schleswig-Holstein, Kiel, Germany*
[b]*Julius Wolff Institut, Charité - Universitätsmedizin Berlin, Berlin, Germany*
[c]*Biomechanics Laboratory, University Medical Center Schleswig-Holstein, Lübeck, Germany*
[d]*Sorbonne Universités, UPMC Univ Paris 06, INSERM, CNRS, Laboratoire d'Imagerie Biomédicale, Paris, France*

Objective: To date it is not clear whether Quantitative Ultrasound (QUS) measured at cortical bone can be used to obtain relevant information about bone fragility exceeding the capabilities of radiological measurements like DXA or CT. In a comprehensive study on tibia bone specimens (supported by Elsbeth-Bonhoff-Foundation, Germany) several methods were applied including different ultrasonic measurements, CT and material testing. In this analysis we concentrated on axial transmission and CT-measurements, which also are applicable in vivo, to investigate whether QUS could add relevant information in patient fracture risk assessment.
Methods: We investigated how axial transmission QUS measurements and bone mineral density (BMD) measured in the midshaft of tibia specimens correlate with ultimate stress of cuboids cut from similar bone regions. Axial transmission measurements were performed using the BDAT device (LIP, Paris) at the anterior part of the tibia. The BDAT probe was positioned at the midshaft parallel to the long axis. Through perpendicular shifting 4 measurement sites were selected covering the complete anterior region of the midshaft. Rectangular specimens were cut from these 4 regions (1 to 5 mm edge length) and tested in compression in axial direction. BDAT speed of sound of the first arriving signal (vFas) and ultimate stress were averaged over the 4 regions. On a slice perpendicular to the midshaft axis, BMD was measured using μ-CT (vivaCT, Scanco Medical). An elliptical measurement region was placed manually in the anterior cortical part.
Results: 16 specimens were included in the study (11 female, 5 male), age 81 +/- 8.6 years. vFas was 3903 +/- 122 m/s, BMD was 929 +/- 73 mg/cm3 and ultimate stress was 144 +/- 27 MPa. vFas correlated with ultimate stress (R^2=0.35, RMSE=21 MPa, $p<0.01$) as did BMD (R^2=0.59, RMSE=18MPa, $p<0.001$). Both variables contributed independently to the estimation of ultimate stress (R^2=0.80, RMSE=13MPa, $p<0.001$) (Figure 1).
Conclusion: These findings indicate that QUS in cortical bone might reflect aspects of bone fragility not captured by BMD. It has to be noticed that geometry and size of the tibia do not have an impact on the measurements of BMD and ultimate stress but on vFas at least in bones of small cortical thickness. Our aim was to explore the contribution of QUS on bone strength excluding size as a confounder. This is only a study with a limited sample size; however, findings are promising and should be verified using a higher number of specimens.

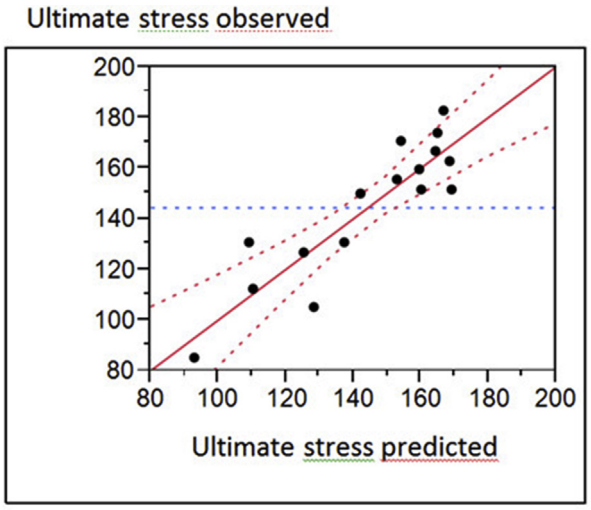

Figure 1: Observed ultimate stress versus predicted

IBDW2014-00166-F0087
STATISTICAL APPEARANCE MODELING OF WHOLE-BODY BONE SHAPE AND DENSITY

Bennett K. Ng [a,b], Louise Marquino [b], Viva W. Tai [c,d], Caitlin Sheets [d], Kathleen Mulligan [c], Timothy F. Cootes [e], John A. Shepherd [a,b]
[a]*University of California Berkeley—University of California San Francisco Graduate Program in Bioengineering, San Francisco, California, United States of America*
[b]*Department of Radiology and Biomedical Imaging, University of California, San Francisco, United States of America*
[c]*Division of Endocrinology and Metabolism, Department of Medicine, University of California, San Francisco, United States of America*
[d]*Clinical and Translational Science Institute, University of California, San Francisco, United States of America*
[e]*Centre for Imaging Sciences, Institute of Population Health, The University of Manchester, Manchester, United Kingdom*

Objective: To model osteoporosis and other bone diseases in terms of their impact on systemic bone shape, size, and density using whole-body DXA imaging and statistical appearance modeling.
Background: To date, osteoporosis has been described using regional DXA bone density assessments (lumbar spine, total hip, neck, etc.) and average values for these regions. Bone shapes have also been studied as additional risk factors (hip axis length, hip structure analysis, etc.). However, these approaches use only a small fraction of the bone shape and density variance observed in a population, and they are indexed by age and development of osteoporosis or other bone-compromising conditions such as diabetes. Statistical appearance modeling (SAM) is a method that captures most of the variance in a set of images in a manageable set of orthogonal variables. Hitherto, SAM has not been applied to whole-body DXA imaging. Our goal is to model 95% of the variance of bone shape and density using SAM. Such a model could improve understanding of how bone form relates to function, and support new hypotheses regarding fracture risk reduction.
Methods: Hologic whole-body DXA images are being acquired on a healthy pilot population. Acquired images were converted into pixel-specific masses of bone, fat, and lean tissue. 102 fiducial points were placed on skin and bone edges using an active appearance modeling software package developed by the University of Manchester. A training subset was used to semi-

automate fiducial point placement. All images were warped to the computed average image by triangulation between adjacent fiducial points. The displacement and mass deviation of each pixel from the corresponding pixel in the average image was fed into a principal component analysis. Eigenvectors describing 95% of the model variances were created. Within this basis model, coefficient vectors were computed for each DXA image. These values were used in general linear models to relate bone shape and density to other facture risk factors.

Results: The modeled fiducial points and triangulation is shown in Figure 1. To date, twenty-one participants have been added to our model. Twenty SAM eigenvectors were derived which capture 99% of the model variance. Seven of these eigenvectors exhibited significant correlations to clinical measures such as height, weight, age, and gender (see Table 1).

Conclusion: This work demonstrates how SAM methods can be used to expand the utility of DXA whole-body images. Further studies are planned using previously-acquired scans for diabetes and fracture risk assessment.

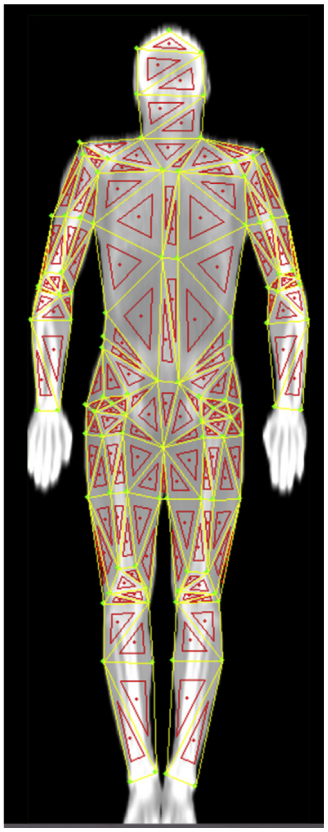

Figure 1: Triangulation of 102 fiducial points placed on whole-body DXA image. Points were defined at landmarks along skin and bone surfaces such that the derived statistical appearance model captures variance in bone shape and density, as well as whole-body shape and composition.

IBDW2014-00167-F0088
VISCERAL FAT MEASURES IN CHILDREN FROM DXA SCAN

John A. Shepherd [a], Bo Fan [a], Xin Ping Wu [b], Michael A. Levine [c]
[a]*Department of Radiology & Biomedical Imaging, University of California San Francisco, USA*
[b]*Institute of Metabolism and Endocrinology,The second Xiangya hospital of central South University, Changsha, P.R China*
[c]*Division of Endocrinology and Diabetes,The Children's Hospital of Philadelphia, Philadelphia, USA*

Objective: Obesity in adolescence has quadrupled in the last 30 years, heralding the recognition that the volume of visceral adipose tissue (VAT) is a strong risk factor for metabolic diseases. DXA scanners made by both GE-Lunar and Hologic have VAT measurement options, but scanners are not FDA-approved for VAT measurement on subjects below 20 years. We sought to determine how well measurements of VAT in children obtained on GE-Lunar and Hologic systems agree. Our criterion for success was whether the relationship between the systems was similar in both kids and adults.

Methods: We were unable to identify a dataset for absolute accuracy studies containing both abdominal CT (or MRI) scans with tomographic analysis plans normal to the table as well as time-registered DXA scans. We used a sample of convenience of 84 children (37 girls, 47 boys) with ages ranging from 6 to 19 years who had been scanned on both GE-Lunar (Prodigy, version 14.0) and Hologic (Apex, version 4.0) systems. In addition, 109 adults (97 women) were scanned on the same two systems.

Results: 10 children (5 girls and 5 boys) had unmeasurable VAT volume results with the GE-Lunar system and were excluded from the agreement analysis. Otherwise, the Hologic VAT measures ranged from 38.8 to 777.9 in kids and 73.9 to 1031.7 in adults. Without adjustments, the association was $R2=0.67$ and 0.88 for kids and adults. With adjustments for android fat and sex, the correlation between GE-Lunar and Hologic VAT volume results were $R2=0.84$ and $R2=0.91$ for kids and adults, respectively. In both adults and kids, VAT was not significantly correlated with age or height, but was significantly correlated to weight, android fat and lean. The RMSE in these adjusted agreements were 117.4 (Hologic to GE-Lunar) and 38.4 (GE-Lunar to Hologic) and 165.3 (Hologic to GE-Lunar) and 67.7 (GE-Lunar to Hologic) for kids and adults.

Conclusion: VAT accuracy between manufactures is similar for kids and adults. The differences are believed to be mainly due to the limited range and low average value of VAT in the kids.

IBDW2014-00168-F0089
NOISE MEASUREMENT AND MODELING ON DEXA DEVICES

F. Michelet, R. Winzenrieth
Med-Imaps, R&D department, Merignac, France

Objective: the goal of this study is to evaluate and quantify noise in images obtained from DXA devices, and to mathematically describe the influence of soft tissues on noise quantity in the final DXA image.

Methods: We used a custom-made noise target made from flat aluminum plates of various thicknesses (to simulate bone) and of HDPE and PVC plates (simulating soft tissues at a desired thickness). We used aluminum thickness ranging from 0mm to 14mm and tissue thickness ranging from 8cm to 20cm and fat percent from 25% to 100%.This noise target was scanned on 4 DXA devices, 2 devices of model A and 2 of model B. We used the usual scan mode

IBDW2014-00166-F0087: Table 1 Pearson product-moment correlations of selected clinical measures to twenty principal components from the active appearance model derived from whole-body DXA images. Highlighted values are statistically significant ($P<0.05$).

Measure	PC0	PC1	PC2	PC3	PC4	PC5	PC6	PC7	PC8	PC9	PC10	PC11	PC12	PC13	PC14	PC15	PC 16	PC17	PC18	PC19
Weight	0.31	-0.20	0.59	0.30	0.08	0.38	0.13	-0.17	-0.14	-0.25	0.14	-0.03	0.00	0.08	0.13	-0.06	0.02	0.03	-0.17	-0.10
Height	-0.14	-0.73	0.35	0.27	0.26	0.29	0.01	-0.06	-0.16	-0.14	0.08	-0.02	0.09	-0.03	0.06	0.00	0.00	0.04	-0.02	-0.18
Whole-body %fat	0.70	0.40	0.20	-0.18	-0.12	-0.24	0.19	-0.13	-0.06	0.14	0.09	0.23	0.05	-0.01	-0.03	-0.28	0.07	0.14	0.04	0.07
Whole-body BMC	-0.04	-0.61	0.38	0.23	0.41	0.27	-0.01	-0.12	-0.08	-0.16	-0.07	-0.20	-0.07	0.14	0.14	0.07	0.04	0.04	-0.19	-0.12
Whole-body BMD	-0.01	-0.44	0.33	0.11	0.45	0.29	-0.07	-0.24	0.08	-0.16	-0.20	-0.23	-0.20	0.20	0.22	0.10	0.14	0.04	-0.26	-0.05
Body volume	0.37	-0.18	0.60	0.30	0.07	0.36	0.16	-0.15	-0.15	-0.22	0.13	-0.02	-0.03	0.08	0.09	-0.11	-0.02	0.01	-0.14	-0.04
Trunk-to-leg volume ratio	0.06	0.07	-0.03	0.48	-0.25	0.39	0.30	0.10	-0.45	0.12	0.14	0.17	0.00	-0.23	-0.02	-0.20	-0.03	0.10	0.31	0.17
Age	0.32	0.24	0.22	0.09	0.03	0.22	0.23	-0.13	-0.09	0.33	0.19	0.05	0.29	-0.05	-0.34	0.05	-0.16	-0.22	0.47	-0.10
Gender	-0.52	-0.38	-0.02	0.52	0.24	0.40	0.09	-0.11	-0.10	-0.03	0.04	-0.02	-0.03	-0.09	0.12	0.19	-0.20	-0.18	0.02	-0.01
Waist circumference	0.39	-0.13	0.55	0.35	0.00	0.27	0.19	-0.12	-0.10	-0.23	0.14	0.08	0.01	0.05	-0.04	-0.07	-0.03	0.35	-0.14	0.15
Hip circumference	0.65	0.12	0.55	-0.09	0.16	-0.06	0.09	-0.15	-0.11	-0.13	-0.07	0.12	-0.10	-0.03	0.01	-0.19	0.14	-0.22	-0.07	-0.06